

# We are IntechOpen, the world's leading publisher of Open Access books Built by scientists, for scientists

6,900

Open access books available

186,000

International authors and editors

200M

Downloads

Our authors are among the

154

Countries delivered to

TOP 1%

most cited scientists

12.2%

Contributors from top 500 universities



WEB OF SCIENCE™

Selection of our books indexed in the Book Citation Index  
in Web of Science™ Core Collection (BKCI)

Interested in publishing with us?  
Contact [book.department@intechopen.com](mailto:book.department@intechopen.com)

Numbers displayed above are based on latest data collected.  
For more information visit [www.intechopen.com](http://www.intechopen.com)



# Flow and Heat Transfer in Jet Cooling Rolling Bearing

*Wei Wu, Jibin Hu and Shihua Yuan*

## Abstract

The real flow field inside a jet cooling ball bearing is an air-oil two-phase flow since the air entrainment in the lubricant is ineluctable. The flow heat transfer characteristics are thought to have significant impacts in cooling effect forecast and temperature control. To this end, the fluid flow and heat transfer characteristics of the air-oil two-phase flow inside a jet cooling rolling bearing have been investigated by simulation and experiment herein. A multiphase VOF numerical method for the flow field calculation has been proposed. The temperature distributions of the bearing system have been measured, and the flow pattern under different operation speeds has also been captured. The parameter effects on the jet cooling rolling bearing flow field and temperature distribution have been revealed accordingly. The research findings can be used for the structural optimization and the precise lubrication design of the rolling bearing.

**Keywords:** ball bearings, jet cooling, two-phase flow, VOF, flow pattern, temperature distribution

## 1. Introduction

Rolling bearings are the most widely used bearings in the vehicle transmission industry due to their advantages of less friction coefficient for rotatory movements [1]. With the future trends of vehicle transmission development shifting toward lighter and more compact designs with greater power density, the main shaft bearings are subjected to more severe demands of simultaneous shrinking size and excessive loading [2, 3]. These requirements enforce higher thermal load on the bearings. The rolling bearings under stress overload and poor heat dissipation conditions are prone to wear out easily due to metal-to-metal contact, which corrode surface of bearings.

Hence, lubrication of bearings plays a significant role in fatigue life assurance by reducing friction and wear, which ensure the safe and reliable operation of bearings. The choice of lubrication mode of rolling bearing mainly depends on load, working speed, and temperature. Grease and splash lubrication are capable enough for low-speed rolling bearings [4], while oil-jet lubrication could better meet the requirements under heavy load, high-speed, and high-temperature conditions [5].

Fluid jet heat transfer enhances the heat transfer rates in comparison with conventional methods. In an oil-jet cooling rolling bearing, a portion of the oil is utilized to lubricate the ball bearing and form lubricant film in ball raceway

contacts. A larger film thickness is helpful to reduce the friction and the heat generation. However, for the high-speed operation, the total energy dissipated by friction is significant, leading to an excessive heat generation. To compensate for this problem, larger amounts of lubricant oil flow are required to provide sufficient cooling capability, while only a relatively small part of the oil is used to form a lubricant film [6, 7]. Besides, while a larger amount of oil mass flow may lead to a higher power loss due to the increased drag against the rotation of the rolling elements and, an insufficient oil mass flow may cause a lubrication failure.

Thus, both the power performance and the lubrication performance of a rolling bearing are considered to be significantly impacted by the flow around it, which is in typical forms of enclosed space flow or open space flow. The enclosed space flow relates to the flow inside a bearing chamber, which is a common flow state in the real operating conditions such as aero engines, etc. However, there is usually no bearing chamber design for the drivetrain applications with lightweight requirements. The flow state of these rolling bearings is an open space flow, in which the heat that determines the temperature of bearing and oil-out is generated by the drag among rolling elements.

Experimental investigations with regard to high-speed ball bearings with oil-jet lubrication have been reported by Zaretsky et al. [8], indicating a lower bearing temperature with a double-nozzle jet construction compared with a single-nozzle jet counterpart under the same given oil flow rate. Flow was simulated using the computational fluid dynamic method for acquiring working performance of the oil-mist lubrication, without and with the flow inside the rolling bearing [9, 10]. The results indicate that the opening near the inner raceway is expected to be the excellent location for supplying oil-mist or oil-jet for accomplishing better lubrication and cooling of ball bearing components. Both the flow pattern around one sphere and its drag coefficient are modified when placing another sphere in its vicinity.

The lubrication performance of the rolling bearing has been investigated a lot by single-phase method [11, 12]. The bearing temperature forecast model, considering the heat transfer of the oil flow and the air flow, respectively, is mainly presented by Harris [13, 14]. The convective heat transfer coefficients are given considering the lubricant oil flow and the air flow, respectively [15]. A computer program Shaberth has been used to calculate the thermal performance of ball bearings [16]. The oil volume fraction is required for input in Shaberth, and an empirical equation was derived for the oil volume fraction value inside the ball bearing as a function of oil flow rate, shaft speed, and bearing pitch diameter. However, the flow field inside a rolling bearing with oil-jet lubrication, in reality, is far more complicated since the air entrainment in the lubricant is ineluctable while the bearing is rotating. In addition, the air flow phase and the lubricant flow phase constantly interact with each other, and their interaction is strongly affected by the rotary speed of the bearing.

As stated above, while an accurate assessment of the flow around the ball bearing is of particular importance, the experiment measurements are not enough, and the numerical studies are mainly based upon single phase and empirical equation which are incapable in reflecting the real physics. This work herein investigates the air-oil two-phase transient flow inside the ball bearing. A CFD modeling method is presented for the air-oil two-phase flow inside the rotary ball bearing. It aims to increase the understanding of the temperature effects and flow pattern of the flow field inside the oil-jet lubricated ball bearing. The results can be used to optimize the precise oil-jet lubrication design to control the amount of lubricant oil inside the ball bearing at a later stage.

## 2. Oil-jet cooling mechanism and experimental setup

Lubrication and cooling are important for the rolling bearing fatigue life extension. It is good for the bearing temperature control. The fluid jet is an effective cooling method which has been used widely in heat dissipation. In the rolling bearing operation, the oil-jet method is used for very high-speed conditions. The number of nozzles, the jet velocity, and the oil flow rate are significant to satisfy the bearing lubrication requirement. In order to overcome the detrimental centrifugal effects in high-speed applications, the lubricant oil under pressure is directed at the side of the bearing. The jet velocity should be sufficiently high since the air surrounding the bearing causes the oil to be deflected from the inner ring. Further, a sufficient amount of lubricant oil should be supplied to the bearing. However, an excessive amount of lubricant oil will increase the bearing temperature unnecessarily.

**Figure 1(a)** shows the schematic configuration of the oil-jet lubrication ball bearing under investigation. The cooling oil is injected into the bearing raceway through a small-diameter nozzle to lubricate and cool the bearing and ensure the safe and reliable operation of the rolling bearing. The high-speed oil-jet atomizes into droplets which then mix with the surrounding air to form a two-phase mixture. Besides, the two-phase mixture is working in an open space environment that has a direct contact with air of the outlets. In this way, coexistence of oil and air two-phase flow is formed inside the ball bearing.

In the high-speed operation of bearings, a large amount of heat generated by friction between moving pairs will lead to bearings and their adjacent parts. A sharp increase of friction heat will lead to a significant increase in the working temperature. If the heat not effectively discharged, it will inevitably lead to the failure of bearings, which will damage the service life of the bearings. The three major heat dissipation methods inside the ball bearing are shown in **Figure 1(b)**, including the conduction through solid structures, the convection from solid structures to fluids, and the radiation to surrounding media. The latter one is not taken into consideration since it dissipates a negligible part of heat in the bearing case. When the bearing is in a state of thermal equilibrium, the main factors that impact the bearing temperature are bearing load, speed, oil-in temperature, and oil volume fraction inside the bearing, which indicates that the flow field and heat transfer characteristics between the two-phase flow and solid components have a considerable influence in the bearing temperature. Thus, it is essential to clarify the correlations between the fluid flow and thermal behaviors in oil-jet cooling bearing, in order to

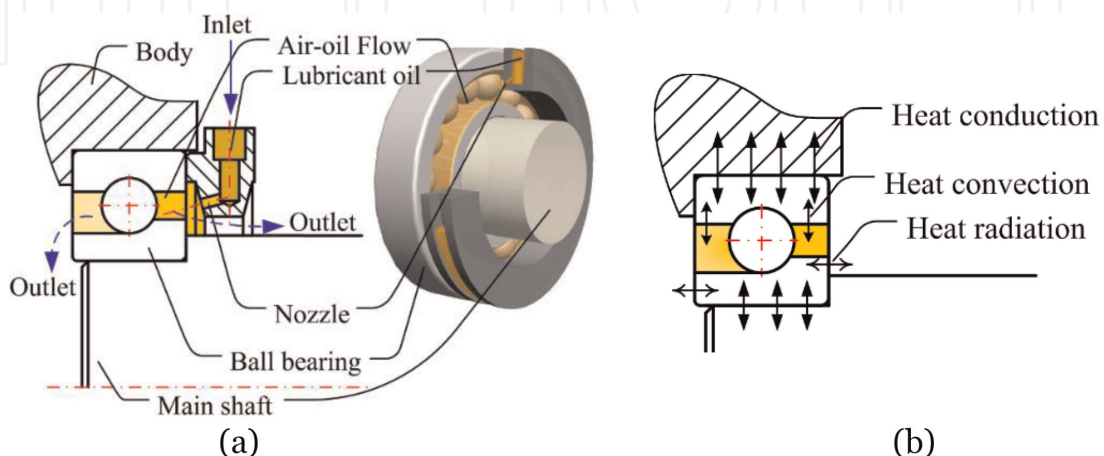


**Figure 1.** Configuration of the oil-jet cooling ball bearing and heat transfer method: (a) configuration of jet cooling mechanism and (b) heat dissipation methods.

make precise assessment of cooling method and optimize the design of cooling devices.

Experiment apparatuses for testing the flow pattern and temperature distribution of the ball bearing have been built up, as shown in **Figure 2**. No load is applied in the flow pattern test, as shown in **Figure 2(a)**. The shaft of the tested ball bearing is horizontal. The maximum tested speed is 4500 r/min which is the rated speed of the driving motor. The parameters of the tested ball bearing are given in **Table 1**. The exact value of the oil volume fraction distribution is difficult to process, since the flow field inside the bearing is compact. Thus, the photograph of the flow pattern is presented to validate the simulated results.

Further, a tested apparatus for temperature test of ball bearing has been built up, as shown in **Figure 2(b)**. The outer ring temperatures of different positions are measured by three temperature sensors.  $r$  is the radial coordinates and  $\omega$  is the circumferential azimuth angle. The technical data of the experimental apparatus is presented in **Table 2**. The measured bearing temperature distribution can be used for computational model validation.

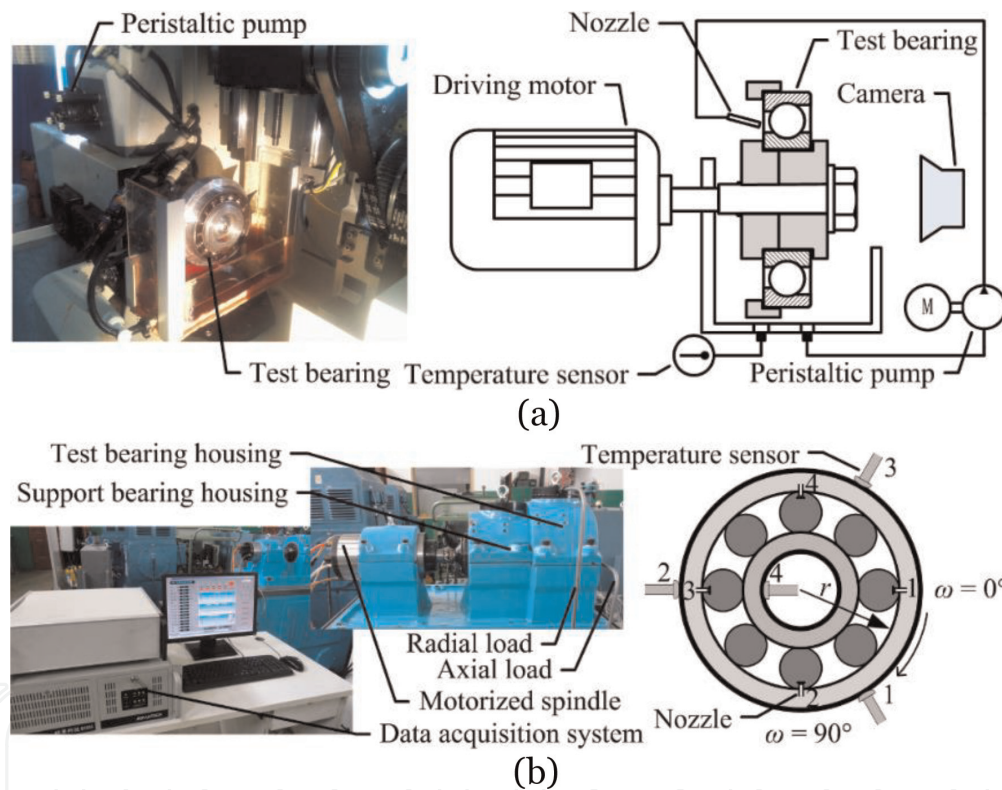


**Figure 2.** Test apparatuses: (a) rolling bearing flow pattern test apparatus and (b) rolling bearing temperature distribution test apparatus.

Quantity	Conversion from Gaussian and CGS EMU to SI
Inner diameter (mm)	50
Outer diameter (mm)	90
Width (mm)	20
Ball diameter (mm)	12.186
Contact angle (deg.)	40

**Table 1.** Specifications of the test ball bearing.

Apparatus and sensor	Technical data
Motorized spindle	0–15,000 r/min
Temperature sensor	Pt1000 (–70 to 500°C)
Oil flow transducer	FT-110 (1.0–10 L/min)
Vibration transducer	JHT-II-B ( $\pm 15$ g)
External radial force	Hydraulic loading (0–30 kN)
External axial force	Hydraulic loading (0–30 kN)

**Table 2.**  
 Technical data of the test apparatus.

### 3. Mathematical modeling

Since the two-phase flow changes constantly in high-speed rotating rolling bearings, the development of a computational fluid dynamics (CFD) model with a two-phase flow method to determine the amount of lubricant oil is of practical value as a substitution of empirical correlations. The volume of fluid (VOF) model is selected to model the two-phase interactions inside the bearing for its recognized ability in tracking the air-oil interface. The two-phase coexistence of the bearing is in the turbulent state. The RNG k- $\epsilon$  model is an economical turbulent model for the rotating or swirling flows, so it is chosen as the turbulent governing equations.

#### 3.1 Governing equations

The oil is defined as the primary phase in the two-phase calculation, and its volume fraction in each cell is denoted as  $\varphi_{oil}$ , with  $\varphi_{oil} = 1$  representing a pure oil phase and  $\varphi_{oil} = 0$  representing a pure air phase. If  $0 < \varphi_{oil} < 1$ , the cell of interest is in the air-oil two-phase state. If the air volume fraction is similarly denoted as  $\varphi_{air}$ , then the sum of the volume fractions of the two phases in the flow domain should meet the follow the constraint:

$$\varphi_{oil} + \varphi_{air} = 1 \quad (1)$$

The properties of an air-oil two-phase flow in the VOF method are treated as the volumetric average of that of the individual phase. Thus, the density, dynamic viscosity, and thermal conductivity are expressed as

$$\rho = \varphi_{oil}\rho_{oil} + \varphi_{air}\rho_{air} \quad (2)$$

$$\mu = \varphi_{oil}\mu_{oil} + \varphi_{air}\mu_{air} \quad (3)$$

$$k = k_{oil}\alpha_{oil} + k_{air}\alpha_{air} \quad (4)$$

where  $\rho_{oil}$  is the oil density,  $\rho_{air}$  is the air density,  $\mu_{oil}$  is the oil dynamic viscosity,  $\mu_{air}$  is the air dynamic viscosity,  $k_{oil}$  is the oil thermal conductivity,  $k_{air}$  is the air thermal conductivity, and  $k_f$  represents the effective thermal conductivity of the two-phase flow.

The governing equations for the entire computational domain are as follows:  
 Continuity equation

$$\nabla \cdot (\rho \vec{v}) = 0 \quad (5)$$

Momentum equation

$$\nabla \cdot (\rho \vec{v} \vec{v}) = \nabla \cdot \left( \mu \left( \nabla \vec{v} + (\nabla \vec{v})^T \right) \right) - \nabla \cdot p + \rho \vec{g} + \vec{F} \quad (6)$$

Energy equation for the fluid

$$\nabla \cdot [\vec{v}(\rho E)] = \nabla \cdot (k_f \nabla T) \quad (7)$$

where

$$E = \frac{\alpha_{\text{oil}} \rho_{\text{oil}} E_{\text{oil}} + \alpha_{\text{air}} \rho_{\text{air}} E_{\text{air}}}{\alpha_{\text{oil}} \rho_{\text{oil}} + \alpha_{\text{air}} \rho_{\text{air}}} \quad (8)$$

Energy equation for the solid

$$\nabla \cdot (k_s \nabla T) = 0 \quad (9)$$

where  $\vec{v}$  is the velocity vector,  $p$  is the pressure,  $\vec{F}$  is the external force,  $\vec{g}$  is the gravity acceleration,  $T$  is the temperature,  $E$  is the energy, and  $k_s$  is the thermal conductivity of the solid structure which varies with different material types.

In order to model fluid turbulence of high-speed swirl inside the bearing, the RNG k- $\epsilon$  model is selected for it is a recognizable model for rotating or swirling flow. The RNG k- $\epsilon$  turbulence model is a model derived from the transient N-S equation using the renormalization group method. Its k equation and  $\epsilon$  equation have the similar form with the standard k- $\epsilon$  turbulence model but are more accurate in calculating the flow field with larger velocity gradient and strong rotational flow by increasing an additional term that is more responsive to the rapid curvature of strain and streamlines.

The transport equation of the turbulence kinetic energy k is

$$\frac{\partial(\rho k)}{\partial t} + \frac{\partial(\rho k u_i)}{\partial x_i} = \frac{\partial}{\partial x_i} \left[ \alpha_k \mu \frac{\partial k}{\partial x_i} \right] + G_k + \rho \epsilon \quad (10)$$

The transport equation of the turbulence dissipation rate equation  $\epsilon$  is

$$\frac{\partial(\rho \epsilon)}{\partial t} + \frac{\partial(\rho \epsilon u_i)}{\partial x_i} = \frac{\partial}{\partial x_i} \left[ \alpha_\epsilon \mu \frac{\partial \epsilon}{\partial x_i} \right] + \frac{C_{1\epsilon} \epsilon}{k} G_k - C_{2\epsilon} \rho \frac{\epsilon^2}{k} \quad (11)$$

where  $G_k$  is the production term of the turbulent kinetic energy caused by the average velocity gradient.  $x_i$  and  $u_i$  represent the coordinate directions and the velocity components, respectively.  $C_{1\epsilon}$ ,  $C_{2\epsilon}$ ,  $C_\mu$ ,  $\alpha_k$  and  $\alpha_\epsilon$  are the turbulence model constants.

### 3.2 Grid meshing

Before the numerical solution of the governing equations, it is important to determine the computational domain and mesh the domain. In order to improve mesh quality and reduce the computer consumption, the computational domain should be simplified and reasonably divided before meshing. **Figure 3** shows the relevant grid schematic diagram of the computational domain, which contains a fluid domain and a solid domain. The fluid domain comprises the internal area of the nozzle, the bearing, and the outlets as shown in **Figure 3(a)**. The flow field

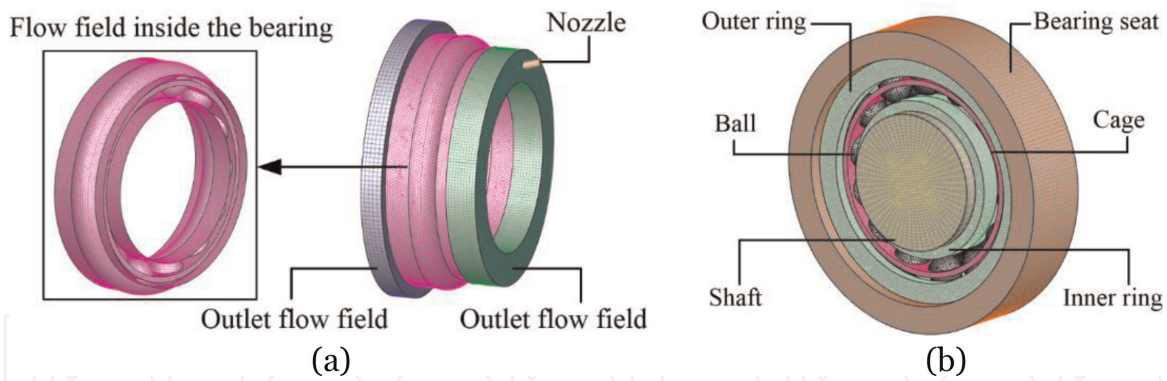


**Figure 3.** Three-dimensional bearing heat transfer grid system: (a) mesh of the fluid domain and (b) mesh of the solid domain.

inside the bearing is the space enclosed by the inner surface of the bearing and the outer surface of the raceway, which is responsible for the most part of the interactions between the fluid flow and the solid elements.

**Figure 3(b)** is the solid domain, which includes the shaft, the rolling elements, the inner ring, the outer ring, the bearing seat, and the cage. The structured hexahedral mesh is used in the areas with regular shapes, such as the inner ring, the outer ring, the bearing seat, and the flow area inside the nozzle, and both of the outlets, etc., in contrast, for areas with relatively complex shapes, such as the flow field inside the bearing, was divided by a tetrahedral unstructured mesh.

The rotation of air-oil flow around the bearing rings is imposed by the rolling elements and the cage, which is rotating at a constant speed, which can be calculated by

$$n_b = \frac{1}{2}n \left( 1 - \frac{D_b \cos \alpha}{d} \right) \quad (12)$$

where  $n_b$  is the rotary speed of the rolling elements,  $n$  is the rotary speed of the inner ring,  $D_b$  is the ball diameter,  $\alpha$  is the bearing contact angle, and  $d$  is the pitch diameter of the bearing.

When setting boundary conditions, the nozzle inlet is initialized with a constant mass flow rate and an initial flow temperature. Flow outlet is set at the end faces of the two outlets and is set to be a pressure outlet boundary condition. The ambient environment is set as 0 Pa gauge pressure and 298 K, respectively. The operating pressure is 101,325 Pa. The viscosity of the oil phase changes with the oil temperature, as shown in **Table 3**. The multiple reference frame (MRF) method is used to describe the rotation of the rolling elements and the flow field inside the bearing. The sliding mesh planes are defined to deal with the interferences between the stationary and rotating computational domains. The heat source was applied to the contact area between the rolling elements and the raceway. Based on the experiment condition, the heat source power was calculated according to Harris's method [13]. Regarding the heat transfer between the fluid and solid structures, both the air and oil heat transfer properties are considered. Coupled heat transfer wall condition

Temperature (°C)	20	40	60	80	100	120
Oil viscosity (Pa·s)	0.305	0.146	0.070	0.034	0.016	0.008

**Table 3.** Variation of the oil viscosity with the temperature.

was set at the solid-fluid interface. The convection coefficients were calculated by following the energy conservation equation in the computation.

### 3.3 Solution methods

The ANSYS FLUENT software platform [17] is used to perform the simulations. The solution format is set as a high-order solution mode. For the VOF air-oil two-phase model, the air phase is set to be the main phase. All the governing equations are discretized by finite volume (FV) method with the second-order upwind scheme and solved by the SIMPLER method.

The residuals and the flux conservation on boundaries, for example, the mass flow rate on inlet and outlet boundaries, are monitored to detect the convergence of the governing equations. The conservation standard is set to be 0.01; that is to say, the computation is considered as convergence, whenever the net mass flow rate between the inlet and outlet boundaries drops to 1% of the mass flow rate on the inlets. Other convergence criteria of residual, such as the volume of fluid function and each velocity component, are all set to be  $10^{-5}$ , except for that of the turbulent kinetic energy and the turbulent kinetic energy dissipation rate which is  $10^{-3}$ .

The criteria are given as follows:

$$\frac{|m_{\text{inlet}} - m_{\text{outlet}}|}{|m_{\text{inlet}}|} < \varepsilon_m \quad (13)$$

$$\frac{|T_{oj+5000} - T_{oj}|}{T_{oj+5000}} < \varepsilon_T \quad (14)$$

where  $m_{\text{inlet}}$  is the oil mass flow at the inlet,  $m_{\text{outlet}}$  is the oil mass flow at the outlet,  $T_O$  is the outflow temperature, and  $\varepsilon_m$  and  $\varepsilon_T$  are the tolerance of oil mass flow and temperature, respectively. The subscript  $j$  is the iteration number.

In numerical simulation, the mesh density has a great influence on the accuracy and correctness of the calculation results. Choosing the appropriate number of meshes not only save the workload of the computer but also increase the reliability of the calculation results. Therefore, grid independence verification is an indispensable task in the process of numerical computation. To perform the grid independence verification, a set of numerical calculation is carried out on a computer platform with the flowing configuration: Processor-Intel E5540  $\times$  2@2.53 GHz CPU, RAM-16 GB (4GB  $\times$  4), Hard Disk-2 TB, Graphic Card e AMD RADEON HD 6670-2 GB, and Operating system-Windows 7 Ultimate 64-bit.

To determine the appropriate number of grids, three different sets of meshes with 135,929, 287,117, and 554,992 cell faces have been tested, and the outlet oil mass flow rate and the average oil volume fraction of the two-phase flow are obtained, as shown in **Table 4**. The numerical calculations show that with the increase of the number of grids, the variations of the calculated outlet oil mass flow rate and the average oil volume fraction are less than 2%. Considering both

	Total number of cell faces	Outlet mass flow rate (kg/s)	Average oil volume fraction (-)
Mesh 1	135,929	0.04399	0.0107
Mesh 2	287,117	0.04456	0.0103
Mesh 3	554,992	0.04420	0.0106

**Table 4.**  
*Technical data of the test apparatus.*

calculation time and accuracy, the mesh with 135,929 cell faces is selected as a suitable number of grids.

#### 4. Investigations of the air-oil flow distribution

To better understand the interaction between the oil and the bearing components, a high-speed camera is used to photograph the flow field inside the bearing with jet cooling. The test rig is mainly composed of a test bearing, a motorized spindle, a high-speed camera, a parallel light, and a gear pump. The gear pump and the motorized spindle can accurately control the oil flow rate and the inner ring speed, respectively. The variation of the flow field under different operating conditions can be captured by the high-speed camera.

##### 4.1 Visualization of the air-oil flow field

The visualized flow field with the corresponding simulations inside the bearing at three different speeds is shown in **Figure 4**. The cooling oil is injected in a rate of 0.15 l/min from a 0.5 mm nozzle that leads to a jet velocity around 12 m/s. The bearing contrarotates at speeds of 500, 2000, and 4000 r/min, respectively. It is seen that all the rolling elements are evenly covered with the cooling oil, indicating

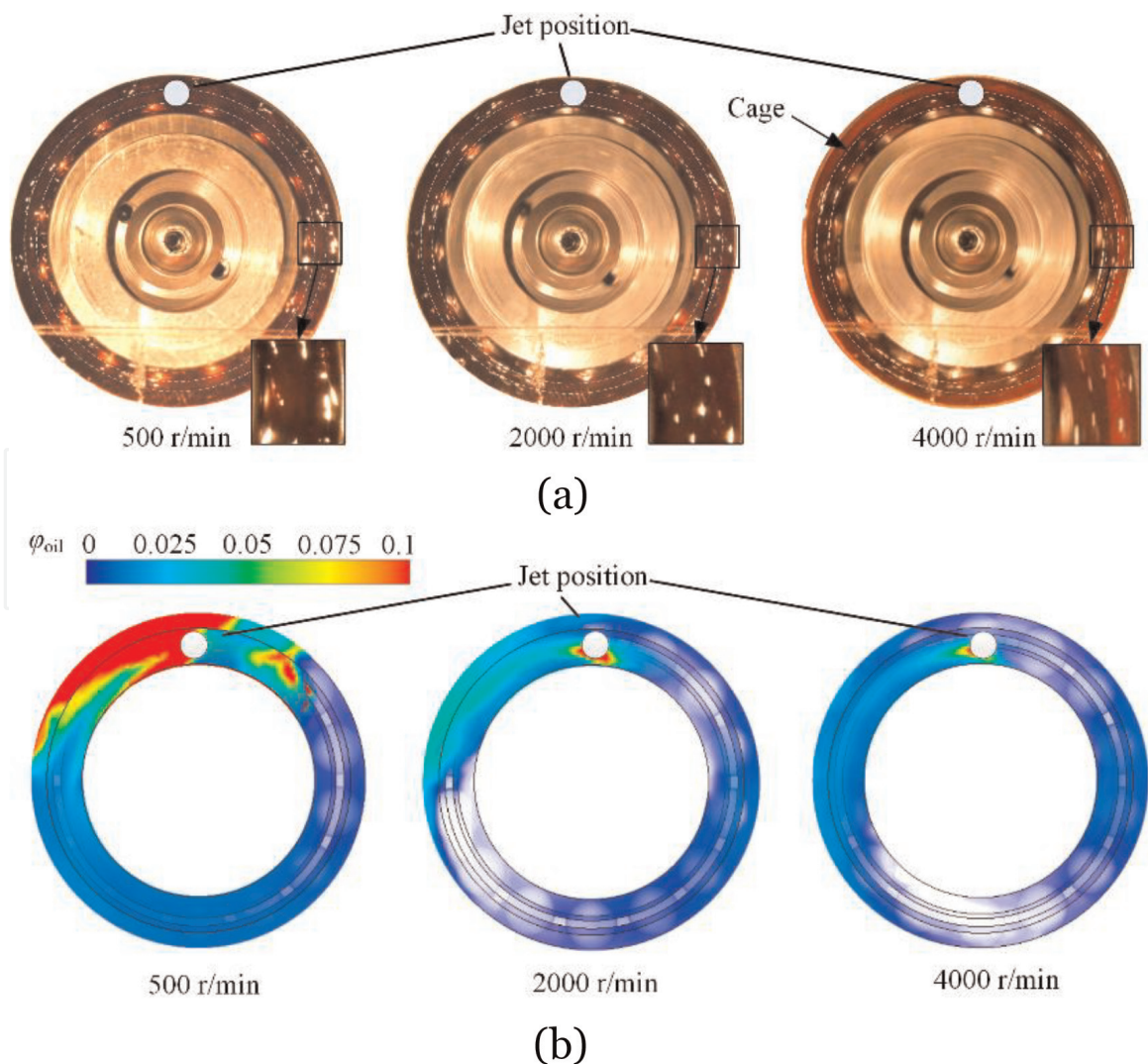


**Figure 4.** Cooling oil distribution at different speeds: (a) measured results and (b) simulated results.

a well-distributed oil film at the speed of 500 r/min. When the bearing speed rotates at 2000 r/min, some of the rolling elements become apparent, indicating a decreased film thickness at a higher speed. Moreover, there are no noticeable bubbles observed inside the cooling oil. As the rotating speed reaches 4000 r/min, rolling elements are seen to be uncovered at certain spots, which indicate an insufficient oil supplement at this condition. Microbubbles, which are evident in the air entrainment, are also observed in this condition.

The contours of oil volume fraction in the simulation results well resemble the visualized flow field at each speed, which again confirms that the oil volume fraction inside the bearing decreases with the increase of bearing rotating speed. Thus, the heat transfer characteristics should be treated as a two-phase flow, especially at higher speeds, since the heat capacities of the oil and air are different.

**Figure 5** represents the visualized and simulated flow field inside the bearing with respect to different flow rates. The bearing again rotates counterclockwise, and the speed is set to be 4000 r/min constantly. With nozzle diameter of 1.5 mm, the test flow rates are 0.3, 0.5, and 0.9 l/min, respectively. The general observation is that, in all tested flow rates conditions, the thickness of the film increases along the outward radial normal direction, which is evidenced by the phenomena that the cooling oil distributes more preferably around the outer ring due to the centrifugal effect.

A further general observation is that the oil film thickness near the outer ring gradually reduces along the direction of rotation under all conditions. For example,

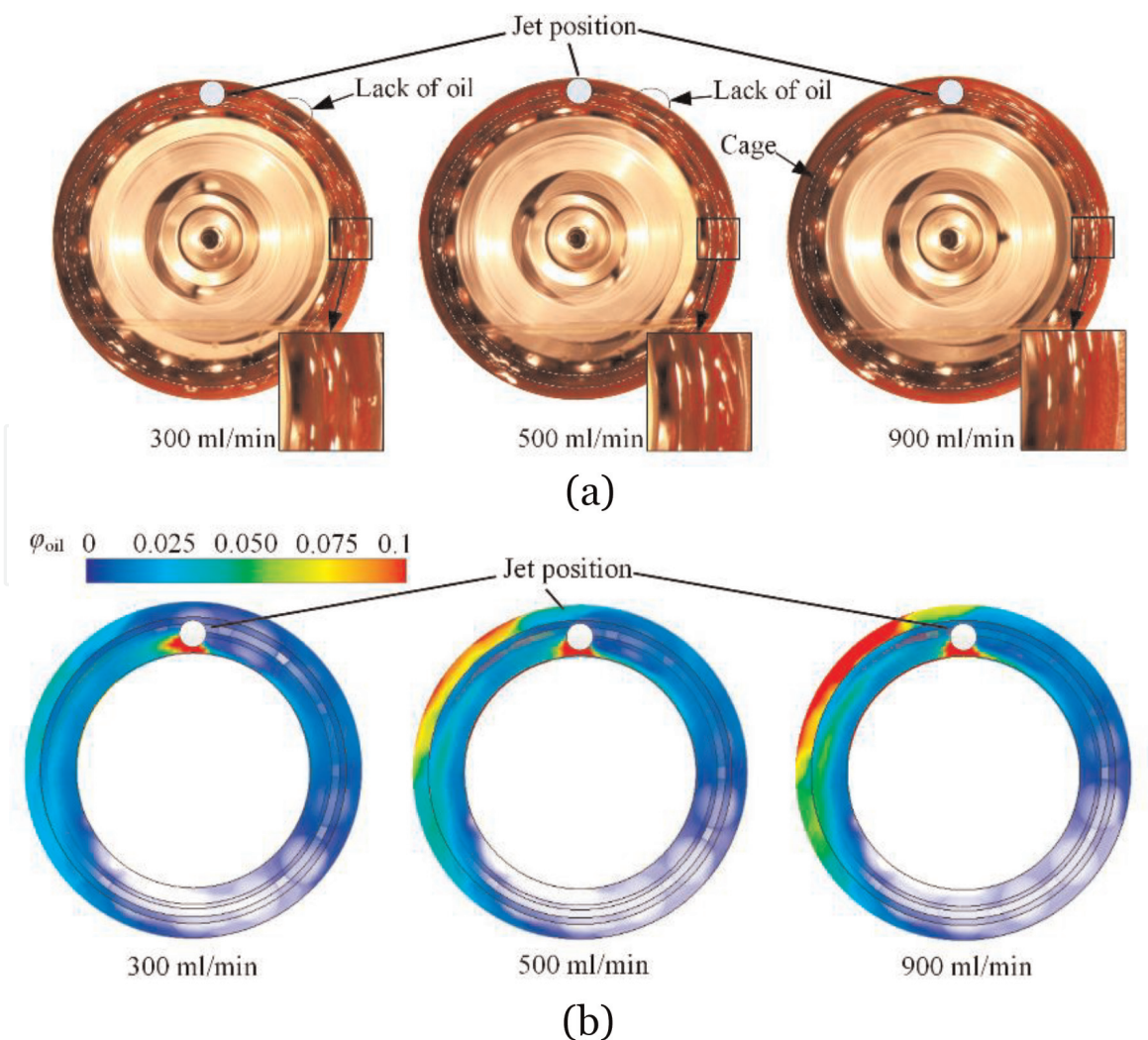


**Figure 5.** Cooling oil distribution at different flow rates: (a) measured results and (b) simulated results.

in the 0.3 l/min case, the oil volume fraction becomes lower along the direction of rotation, and the lowest oil volume fraction appears at the upstream of the jet position, leading to a lack of oil. For the 0.5 l/min case, the oil lack area shrinks at the same observation position, while there is no sign of insufficient oil supplement under the 0.9 l/min condition. This observation indicates that large flow rate is beneficial in homogenization of the cooling oil distribution inside the bearing. Nevertheless, please be noted that the power efficacy could be damaged if an unduly large flow rate of oil is used since the churning loss can be quite high.

**Figure 6** shows oil volume fraction simulations inside the same bearing at high-speed conditions. The cooling oil distributions at different speeds show similar trends, as shown in **Figure 6(a)**. The oil volume fraction reaches its peak value at a certain downstream vicinity of the jet position and gradually reduces along the bearing rotation direction from then on. However, the peak oil volume fraction emerges at random position. The area of the peak oil volume fraction also changes under different speeds, as shown in **Figure 6(b)**. It can be seen that the highest oil

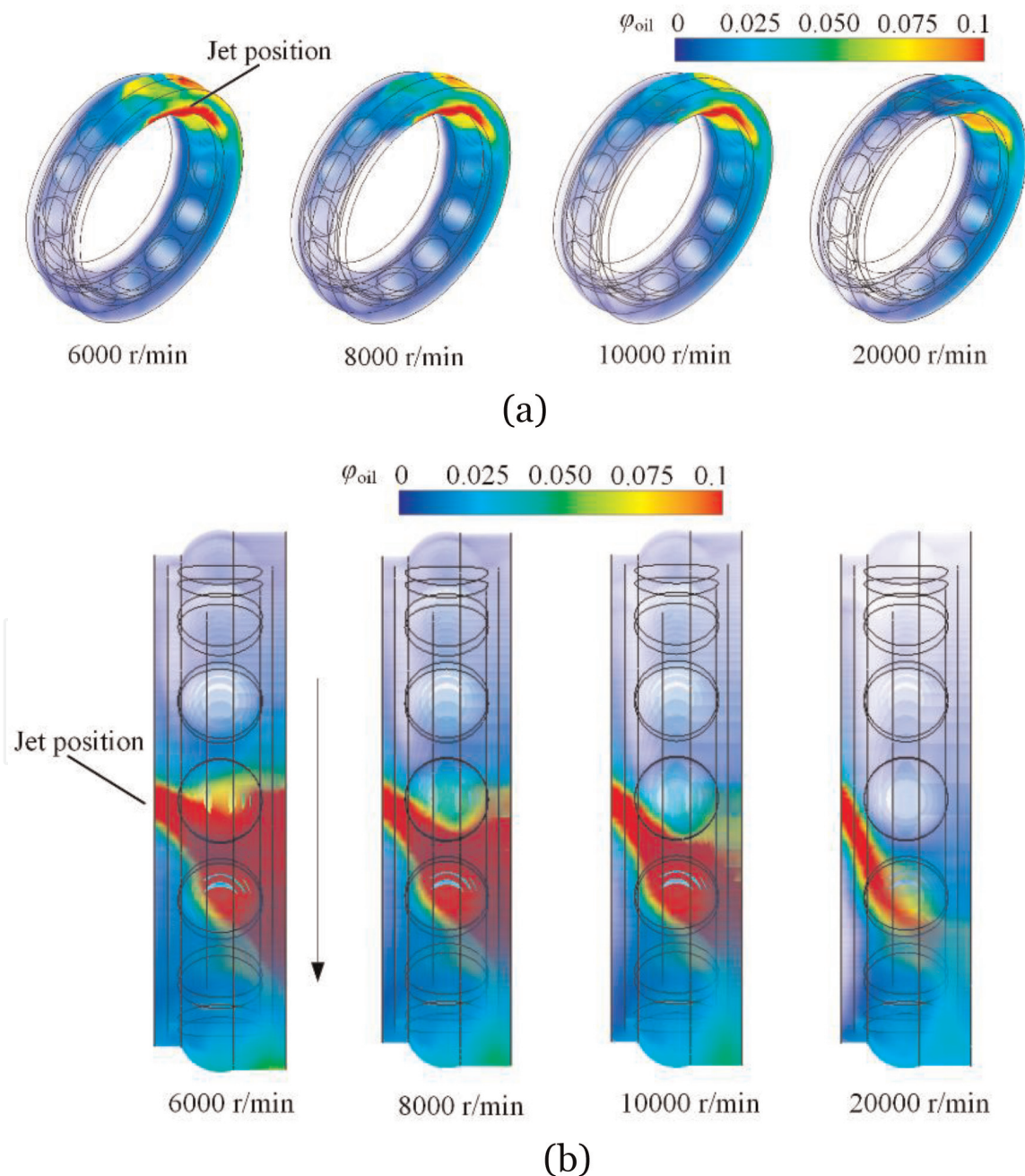


**Figure 6.** Cooling oil flow field at higher speeds: (a) simulated oil flow field and (b) oil flow at the jet position.

volume fraction position moves along the rotation direction. This is because that the circumferential angular velocity of the oil increases rapidly at a higher speed. The oil is driven by the roller and cage. Further, part of the oil passes through the bearing directly at a lower speed. This reduces the utilization efficiency of the cooling oil.

#### 4.2 Parametric studies on the air-oil flow distribution

**Figure 7** shows the calculated air-oil distribution with different nozzle numbers. The speed of the inner ring is 10,000 r/min, and the oil flow rate is 3.0 l/min. The oil volume fraction contours from three to eight nozzles are given in **Figure 7(a)**. It is seen that the oil volume fraction rises with the increase of the nozzle number. **Figure 7(b)** presents the oil volume fraction distribution around the circumference. The parametric results of the oil volume fraction indicate the effect of the different nozzle numbers. It seems that the uniformity of the oil volume fraction inside the bearing rises with the increase of the nozzle number. The oil volume fraction also

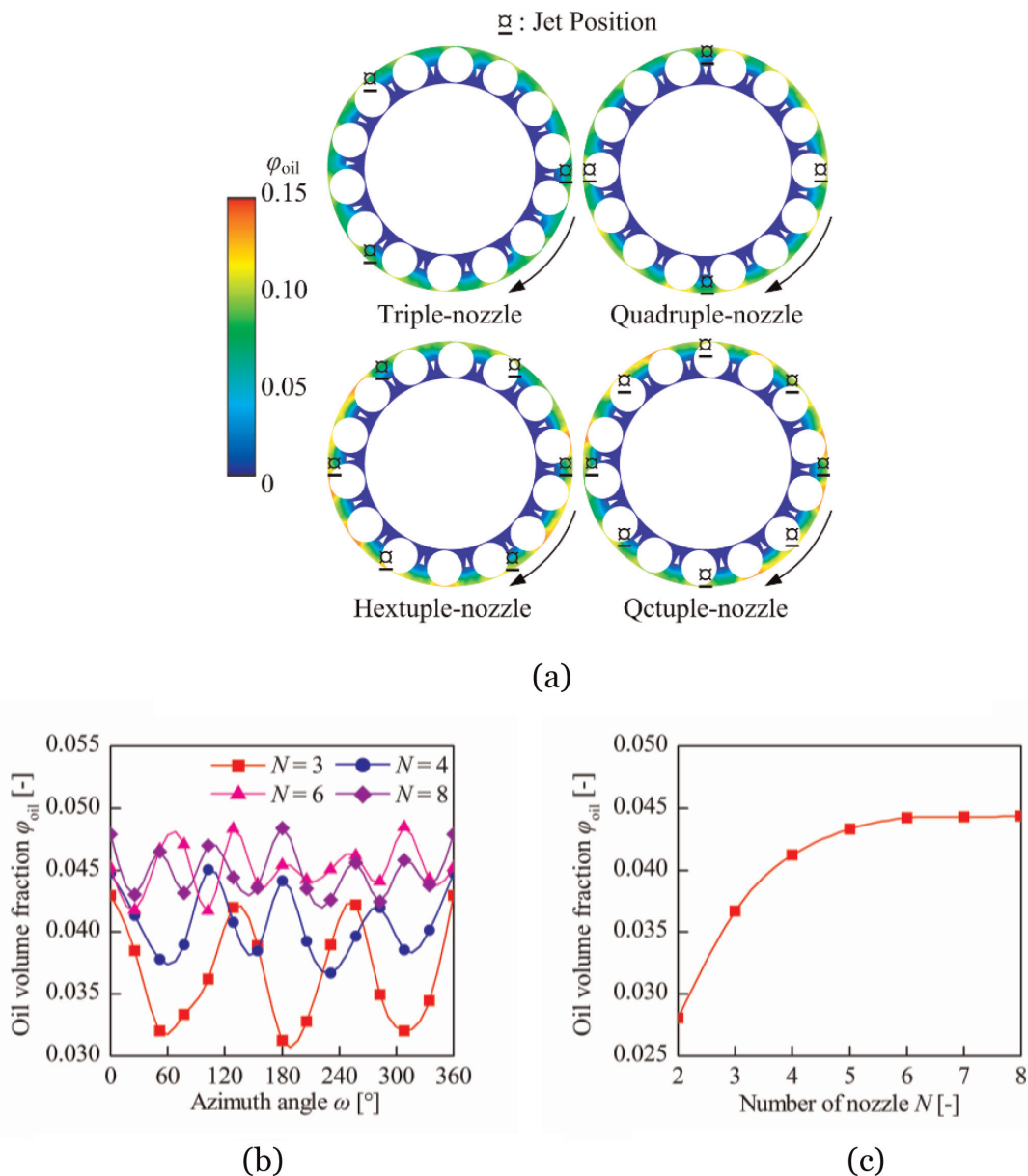


**Figure 7.** Air-oil distribution with different numbers of nozzles: (a) oil volume fraction contours in the center cross section; (b) oil volume fraction distributions; and (c) average oil volume fraction around the circumference vs. the number of nozzle.

increases with the increase of the nozzle number. However, when the nozzle number is larger than 6, the oil volume fraction improvement becomes unapparent, as shown in **Figure 7(c)**. Further, when the nozzle number exceeds 4, the variation of the oil volume fraction and the uniformity of the oil volume fraction inside the bearing are less than 10%, as shown in **Table 5**. The multiple-nozzle jet requires a more complex mechanism than the single-nozzle jet.

**Figure 8** shows the correlations between the air-oil distribution and jet velocity. The rolling bearing with a single-nozzle jet configuration is simulated; the oil volume fraction is obtained under a revolution speed of 10,000 r/min, and the oil flow rate is 3.0 l/min. The oil volume fraction is shown staying around both the inner

Nozzle numbers	1	2	3	4	6	8
Uniformity of the oil volume fraction	1.6029	0.6864	0.3189	0.2830	0.2624	0.2580
Rate of change	—	57.2%	53.5%	11.3%	7.3%	1.7%

**Table 5.**  
 Uniformity of the oil volume fraction with different nozzle numbers.

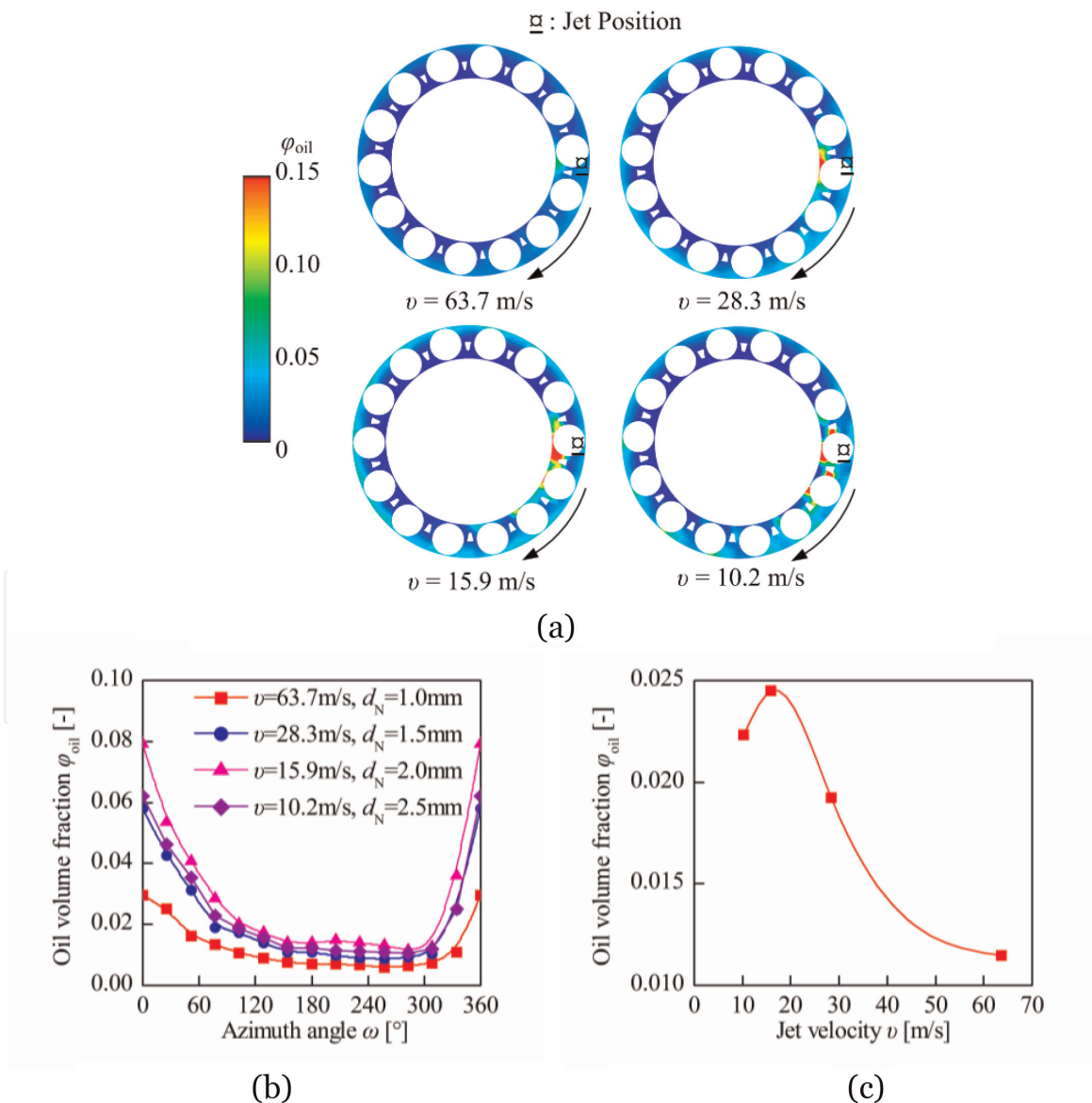


**Figure 8.**  
 Air-oil distribution with different jet velocities: (a) oil volume fraction contours in the center cross section; (b) oil volume fraction distributions; and (c) average oil volume fraction around the circumference vs. the jet velocity.

ring and the outer ring which becomes much lower with the increase of the jet velocity, as shown in **Figure 8(a)**. However, the oil volume fraction becomes more uniform with higher jet velocity. The oil volume fraction distribution around the circumference decreases with the higher jet velocity, as shown in **Figure 8(b)**. However, the jet velocity has little effect on the tendency of the oil volume fraction distributions around the circumference. Further, there is a jet velocity at which the average oil volume fraction achieves the largest value. The calculated result of the jet velocity is between 15 and 20 m/s in the given operation conditions, as shown in **Figure 8(c)**. The detailed relationship between the jet velocity and the oil volume fraction still needs more effort to investigate.

**Figure 9** shows the simulated air-oil distribution with different oil flow rates under a constant speed of 10,000 r/min. As indicated in **Figure 9(a)**, the oil volume

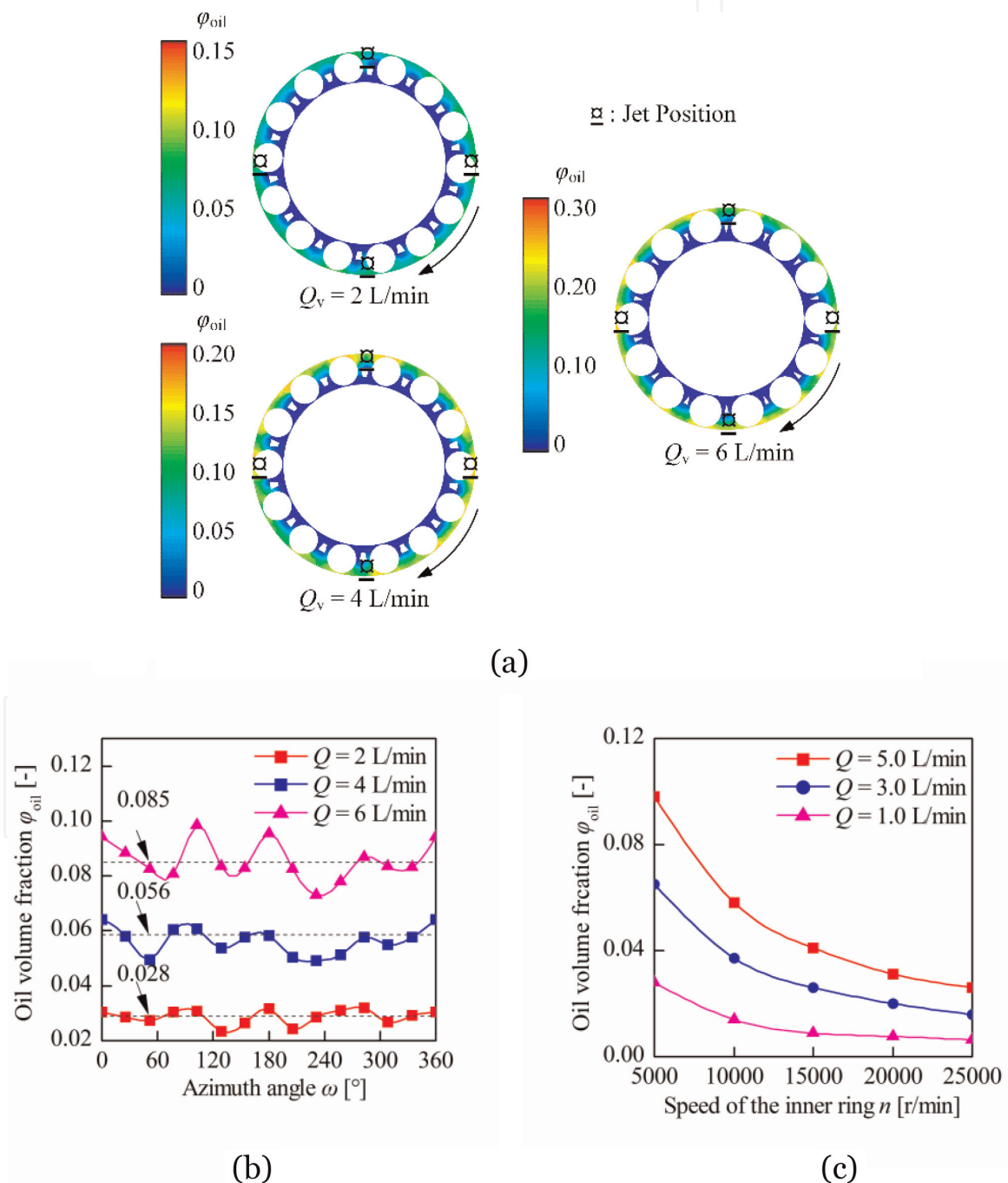


**Figure 9.** Air-oil distribution with different oil flow rates: (a) oil volume fraction contours in the center cross section; (b) oil volume fraction distributions and (c) average oil volume fraction around the circumference vs. the operation speed.

fraction inside the bearing is increased as the oil flow rate increases. **Figure 9(b)** indicates that the oil volume fraction distribution under different oil flow rate condition shows similar trends; however, the amplitude of the oil volume fraction rises with the increase of the oil flow rate. Moreover, the oil volume fraction distributed more evenly at locations far from the jet position. The average oil volume fraction increases with the decrease of the speed, and the increase tendency becomes faster at higher speed, as shown in **Figure 9(c)**. Large flow rate is beneficial in homogenization of the cooling oil distribution inside the bearing and therefore the heat dissipation of the bearing. Nevertheless, the power efficacy could also be damaged due to the resulting unduly churning loss.

## 5. Investigations of the temperature distribution

Tested apparatuses for the temperature distribution of the ball bearing have been built up as shown in **Figure 2**. There are three temperature sensors attached to the outer ring of the test bearing and one more temperature sensor on the inner ring. A data acquisition system is also employed to collect and transmit the data to a computer for further analysis.

### 5.1 Temperature variations of the bearing

**Figure 10** shows simulated outer ring temperature with the consideration of the nonuniform air-oil two-phase distribution under a bearing speed at 10,000 r/min. The oil flow rate is 3.0 l/min, which is equivalent to a jet speed about 10 m/s. The bearing is imposed with an axial load of 5.0 kN in the test. **Table 6** shows the comparison between the test measurements and simulation results. It is shown that the relative tolerance between the tests and the simulations is smaller than 5%,

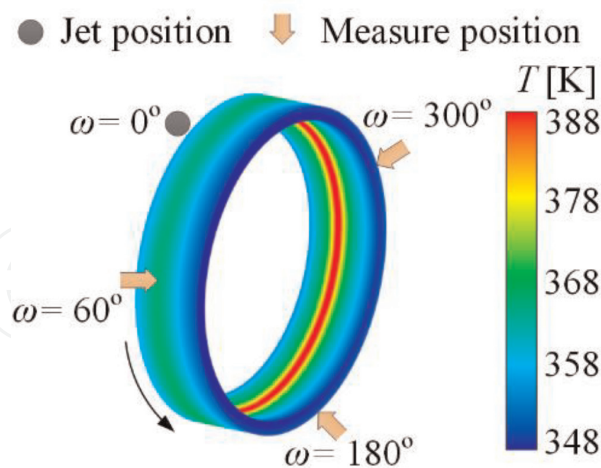


**Figure 10.**  
 The simulated temperature of the outer ring.

Location angle [°]	Simulated value [K]	Measured value [K]	Error (%)
60	365.58	373.6	2.19
180	368.06	376.1	2.18
300	369.23	378.4	2.48

**Table 6.**  
 Measured and simulated outer ring temperatures.

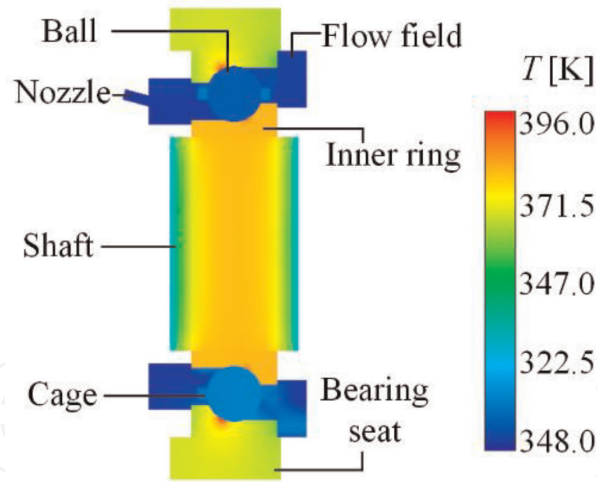


**Figure 11.**  
Temperature distribution of the fluid-solid coupling heat transfer area.

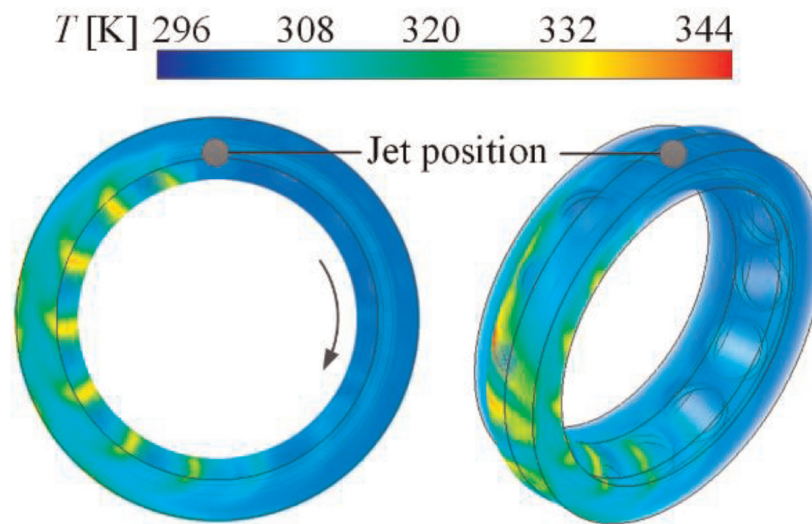


**Figure 12.**  
Temperature distribution of the oil flow field inside the bearing.

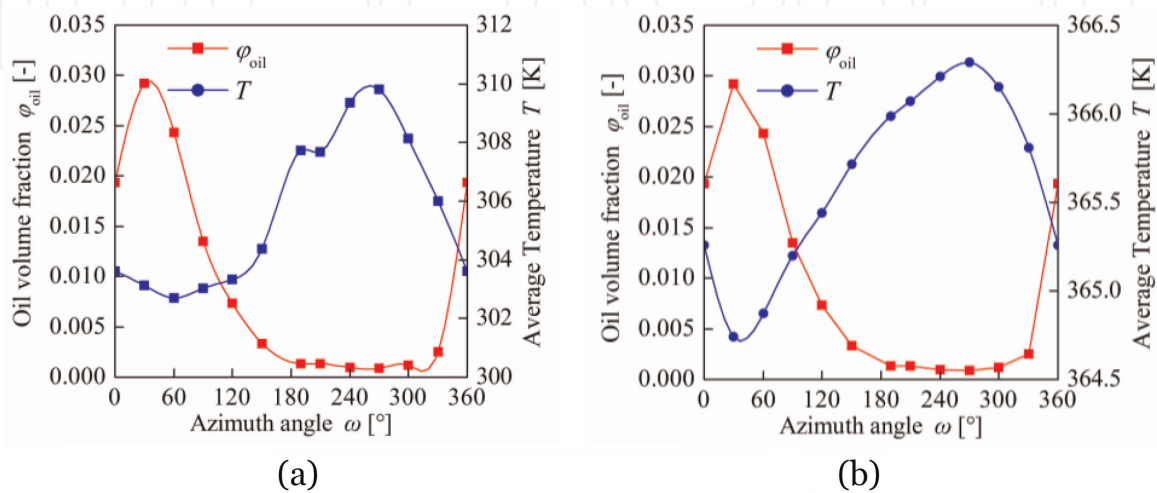


**Figure 13.**  
Simulation of average circumferential temperature and oil volume fraction distributions: (a) average oil temperature and (b) average outer ring temperature.

which indicates that the simulated results are in good agreements with the experimental results and sufficient in performing quantitative analyses, since the research focuses are the overall heat transfer effects of the air-oil flow inside the bearing.

**Figure 11** shows the simulation result of radial temperature distribution of both the fluid and solid domains inside the rolling bearing. The temperature distribution along the radial direction is inhomogeneous. The inner ring shows a relatively high temperature compared to that of the rolling elements. It is reasonable since the distribution of cooling oil around the inner ring is less, as most of the cooling oil is forced to leave the inner ring for the outer ones due to the strong centrifugal effect under high rotating speed. The accumulation of cooling oil near the outer ring surface leads to a better heat transfer effect that contributes to the lower temperature of the outer ring. Owing to the large heat-generating rate between roller and raceway, the temperature in these contact regions is of the highest level.

The 3D display of the simulated temperature distribution shown in **Figure 12** confirms the nonuniformity of the temperature distribution inside the bearing. As shown in **Figure 13**, the temperature distribution of the flow field has a close

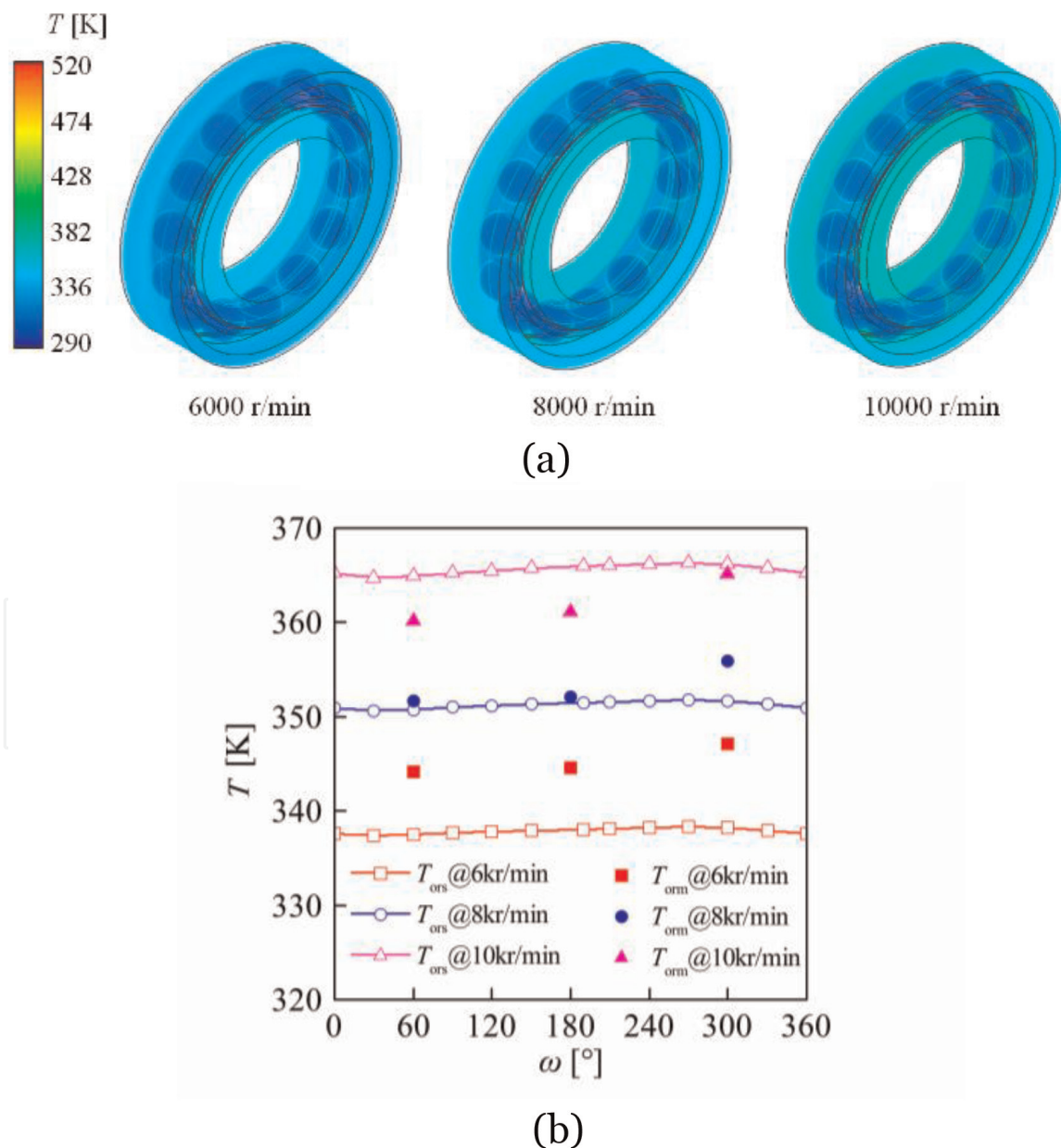


**Figure 14.** The temperature distribution at different speeds: (a) bearing temperature distributions and (b) simulated and measured outer ring temperatures around the circumferential direction.

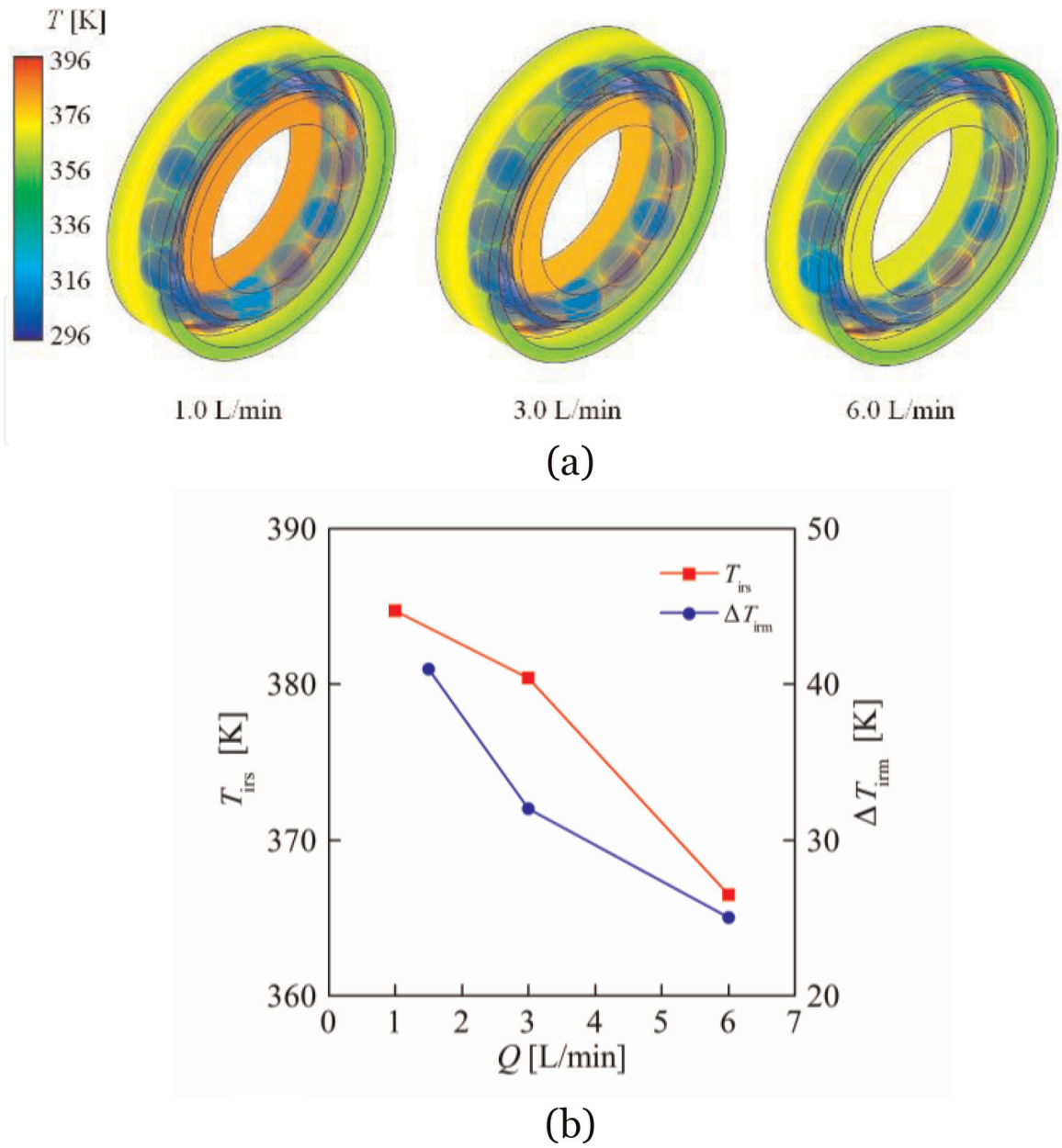


**Figure 15.** The temperature distributions at different oil flow rates: (a) Bearing temperature distributions and (b) simulated inner ring temperature and measured inner ring temperature variations.

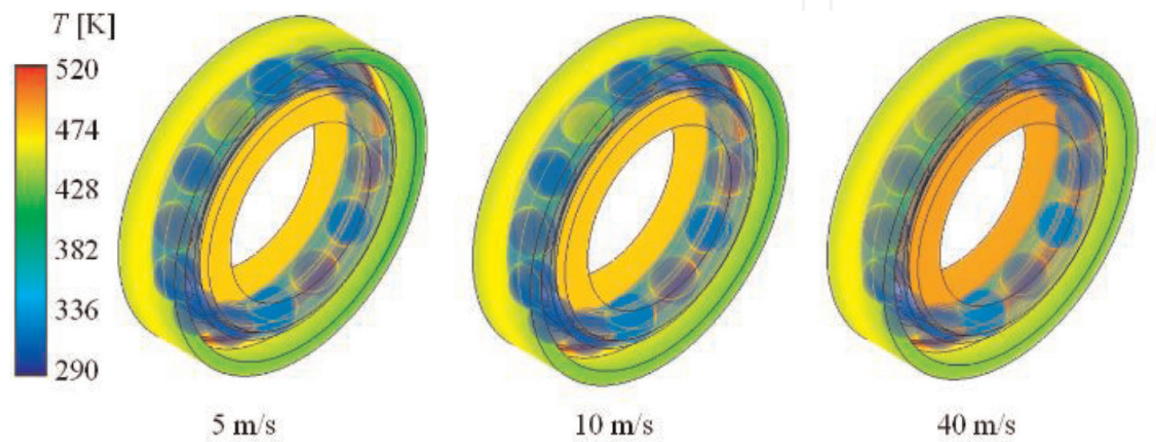


**Figure 16.** The temperature distributions at different oil-jet speeds.

association with the distribution of oil and gas. It is known that the heat transfer capacity of oil is considerably higher than that of air. That explains the reason that the lower temperature always achieves at positions with higher oil volume fractions, such as the positions that are close to the jet position. In general, the temperature near the nozzle is the lowest and increases gradually along the direction of rotation. It drops on the other side of the nozzle. This is because the low-temperature oil is discharged from the nozzle, and the low-temperature oil is constant. More oil supplement is the key factor in achieving better heat convection and lower temperatures.

## 5.2 Parametric studies on the temperature distribution

**Figure 14** shows the temperature distribution of the ball bearing at different speeds. The operating speeds of the bearing are 6000, 8000, and 10,000 r/min, respectively. The flow rate is 3.0 L/min and the oil injection speed is 10 m/s. It seems that the bearing temperature varies obviously at different speeds. With the increase of the speed, the bearing temperature rises, especially at a higher speed. Different from the average circumferential temperature distribution in the internal ring, the circumferential temperature difference exists in the outer ring. Further, the average temperature of the internal ring is higher than that of the outer ring.

**Figure 15** shows the temperature distribution of the ball bearing under different oil flow rates. The oil flow rates are 1, 3, and 6 L/min with a speed of 10,000 r/min. The internal ring rotating direction is clockwise. The result indicates that the oil volume fraction of the flow field increases gradually. The convection heat transfer coefficient of the bearing boundary will also increase correspondingly. The heat dissipation condition becomes better. It is because that the amount of the oil entering the flow field in a unit time increases. At a constant speed, the stirring ability of the roller and cage changes little. Thus, the internal flow field of the bearing is distributed with more oil. The average temperatures of the rings and the flow field decrease, as shown in **Figure 15(b)**.

**Figure 16** shows the temperature distribution of the ball bearing at different jet speeds. The jet speeds are 5, 10, and 40 m/s with an operating speed of 10,000 r/min. The lubrication flow rate is 3.0 L/min. With the increase of the jet speed, the oil volume fraction of the flow field inside the bearing reduces gradually. The temperature of the bearing also rises. The variation of the outer ring temperature is not apparent compared with the inner ring. It is because that the convective heat

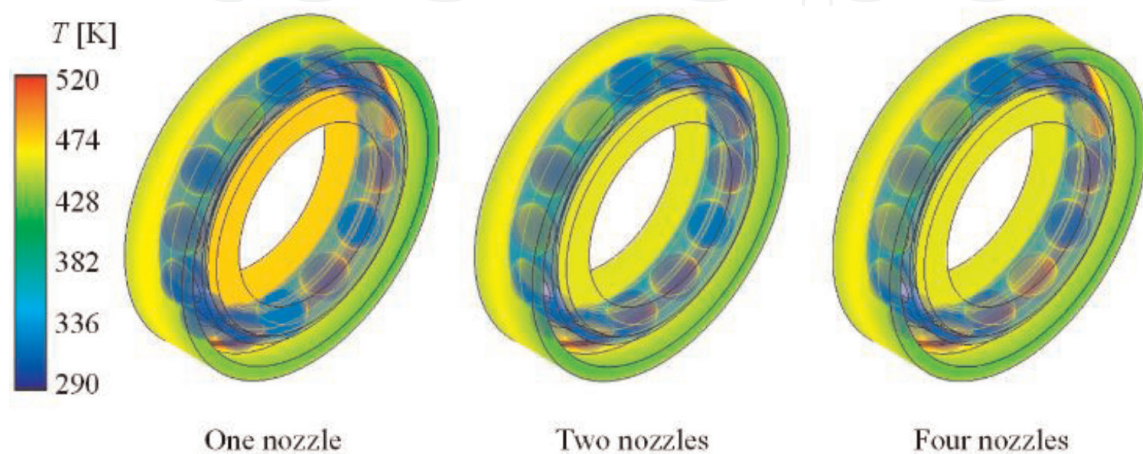


**Figure 17.**  
*The temperature distributions with different nozzle numbers.*

Speed (r/min)	Temperature sensor					
	Outer ring temperature (°C)					
	One nozzle			Two nozzles		
	No. 1	No. 2	No. 3	No. 1	No. 2	No. 3
6000	71.0	71.4	74.0	69.0	68.3	70.3
10,000	87.2	88.1	92.0	84.0	83.7	86.7

**Table 7.**  
The measured temperatures with different nozzle numbers and speeds.

transfer capacity of the bearing boundary decreases, especially around the inner ring. The heat dissipation condition becomes worse with a higher jet speed.

**Figure 17** shows the temperature distribution of the ball bearing under different nozzle numbers. The nozzle numbers are 1, 2, and 4 with an operating speed of 10,000 r/min. The oil-jet speed is 10 m/s and the oil flow rate is 3.0 L/min. The bearing temperature is decreased with a larger nozzle number. The heat convection coefficient inside the bearing increases. The experiments of the bearing with one nozzle and two nozzles have been carried out.

**Table 7** presents the experimental results. The measured temperatures were presented. The axis load is 5 kN and the radial load is 10 kN. It can be seen that the increase of the nozzle number can improve the heat dissipation effect under a constant flow rate. The experimental results are consistent with the calculated results.

## 6. Conclusions

A three-dimensional CFD analysis using the VOF multiphase model has been carried out to study heat transfer and fluid flow behavior in a jet cooling rolling bearing. The nonuniform air-oil distribution and temperature distribution of the two-phase flow inside the bearing had been studied. The results suggest the following:

1. The jet cooling oil inside the ball bearing is not pure oil phase, especially at the high-speed operation. The microbubble is mixed into the oil. The air-oil two-phase flow should be considered in the jet cooling bearing heat transfer analysis.
2. The VOF multiphase model and the coupled boundary conditions can be used to simulate the heat transfer phenomenon of a jet cooling rolling bearing. The influences of the different operation conditions on the bearing component temperatures can be forecasted. The results can be used to guide the design of the lubricating mechanism.
3. The oil volume fraction reaches the highest value at the position close to the nozzle. The highest oil volume fraction position changes with different speeds and moves along the rotation direction.
4. The full wall oil film appears inside the jet cooling bearing at the low-speed stage. It breaks with the increase of the rotating speed. The oil-gas distribution is fairly uniform, and the oil volume fraction is low during the high speed.

5. With the increase of the rotating speed, the bearing temperature increases. With higher flow rate, larger nozzle number, and lower jet speed, the average temperature of the bearing system decreases. The outer ring temperature changes much smaller than that of the inner ring with the variation of the flow rate, nozzle number, and jet speed.

The flow field and thermal behavior analyses give an opportunity for the advanced precision cooling mechanism design of the high-speed rolling bearing. Work on these topics is underway in the National Key Laboratory of Vehicular Transmission at the Beijing Institute of Technology.

### **Conflict of interest**

The authors declared that they have no conflicts of interest with other parties that can unsuitably influence the manuscript entitled “Flow and Heat Transfer in Jet Cooling Rolling Bearing.”

### **Author details**

Wei Wu\*, Jibin Hu and Shihua Yuan  
National Key Laboratory of Vehicular Transmission, Beijing Institute of  
Technology, Beijing, P.R. China

\*Address all correspondence to: [wuweijing@bit.edu.cn](mailto:wuweijing@bit.edu.cn)

### **IntechOpen**

© 2019 The Author(s). Licensee IntechOpen. This chapter is distributed under the terms of the Creative Commons Attribution License (<http://creativecommons.org/licenses/by/3.0>), which permits unrestricted use, distribution, and reproduction in any medium, provided the original work is properly cited. 

## References

- [1] Gloeckner P. The influence of the raceway curvature ratio on power loss and temperature of a high-speed jet engine ball bearing. *Tribology Transactions*. 2013;**56**(1):27-32
- [2] Jiang S, Mao H. Investigation of the high speed rolling bearing temperature rise with oil-air lubrication. *Journal of Tribology-Transactions of the ASME*. 2011;**133**(2):1-9
- [3] Pinel SI, Signer HR, Zaretsky EV. Comparison between oil-mist and oil-jet lubrication of high-speed, small-bore, angular-contact ball bearings. *Tribology Transactions*. 2001;**44**(3):327-338
- [4] Aidarinis J, Missirlis D, Yakinthos K, Goulas A. CFD modeling and LDA measurements for the air-flow in an aero engine front bearing chamber. *Journal of Engineering for Gas Turbines and Power-Transactions of The ASME*. 2011;**133**(8):1-8
- [5] Hu JB, Wu W, Wu MX, Yuan SH. Numerical investigation of the air-oil two-phase flow inside an oil-jet lubricated ball bearing. *International Journal of Heat and Mass Transfer*. 2014;**68**:85-93
- [6] Wu W, Hu C, Hu J, Yuan S. Jet cooling for rolling bearings: Flow visualization and temperature distribution. *Applied Thermal Engineering*. Jul. 2016;**105**(SI):217-224. DOI: DOI. 10.1016/j.applthermaleng. 2016.05.147
- [7] Hager CH, Doll GL, Evans RD, Shiller PJ. Minimum quantity lubrication of M50/M50 and M50/Si3N4 tribological interfaces. *Wear*. 2011;**271**(9-10): 1761-1771
- [8] Zaretsky EV, Signer H, Bamberger EN. Operating limitations of high-speed jet-lubricated ball bearings. *Journal of Lubrication Technology*. 1976;**98**(1): 32-39
- [9] Oh IS, Kim D, Hong SW, Kim K. Three-dimensional air flow patterns within a rotating ball bearing. *Advanced Science Letters*. 2013;**19**(8):2180-2183
- [10] Yann M, Christophe C, Fabrice V. Numerical investigations on drag coefficient of balls in rolling element bearing. *Tribology Transactions*. 2014; **57**:778-785
- [11] Zhou H, Luo G, Chen G, Wang F. Analysis of the nonlinear dynamic response of a rotor supported on ball bearings with floating-ring squeeze film dampers. *Mechanism and Machine Theory*. 2013;**59**:65-77
- [12] Gloeckner P, Ebert F. Micro-sliding in high-speed aircraft engine ball bearings. *Tribology Transactions*. 2010; **53**(3):369-375
- [13] Harris TA, Barnsby RM, Kotzalas MN. A method to calculate frictional effects in oil-lubricated ball bearings. *Tribology Transactions*. 2001;**44**(4): 704-708
- [14] Harris TA, Kotzalas MN. *Rolling Bearing Analysis*. 5th ed. New York: Taylor & Francis; 2006
- [15] Takabi J, Khonsari MM. Experimental testing and thermal analysis of ball bearings. *Tribology International*. 2013;**60**:93-103
- [16] Hirt C, Nichols B. Volume of fluid (VOF) method for the dynamics of free boundaries. *Journal of Computer Physic*. 1981;**39**(1):201-225
- [17] ANSYS Inc. ANSYS FLUENT 15.0 Tutorial Guide. In: ANSYS Inc. 2015